I2MTC 2023 Paper ID: #1570872824

Mass Flowrate Measurement of Slurry Using Coriolis Flowmeters and Data Driven Modelling

Wasif Shafaet Chowdhury, Yong Yan, *Fellow, IEEE*, Marc-Antony Coster-Chevalier, and Jinyu Liu

***Abstract*—Coriolis flowmeters have been proven to be effective while measuring single phase flows, however, the measurement accuracy degrades in case of multiphase flows. This paper presents data-driven models that are incorporated into Coriolis flowmeters for mass flowrate measurement of two-phase (sand-water) slurry. Three different data-driven models based on Support Vector Machine (SVM), Artificial Neural Network (ANN) and Gaussian Process Regression (GPR) are established through training and testing. To examine the behaviors of Coriolis flowmeter for slurry flow measurement, a series of experimental tests were conducted on a purpose-built slurry test rig under a range of mass flowrates (5435 - 18582 kg/h) and Solid Volume Fractions (SVFs) between 0 - 3.3%. The effects of the geometry and orientation conditions of Coriolis measuring tubes are also examined by installing two Coriolis flowmeters on horizontal pipe sections with their measuring tubes in upward and downward orientations. The factors that lead to measurement errors including density difference, asymmetry, damping, Coriolis tube geometry and orientation conditions are practically evaluated. The performances of the SVM, ANN and GPR models are assessed in comparison with the reference readings. A data augmentation technique is also applied to generate unseen condition data with ±5% deviation from the original data. The experimental results show that the GPR models are superior to the SVM and ANN models in terms of measurement accuracy. For the GPR models, 97% and 95.5% of the original data and 99% and 98% of the augmented data yield a relative error within ±0.2% for upward and downward orientations of Coriolis flowmeters, respectively, under all test conditions.**

***Index Terms*— Slurry flow, mass flowrate measurement, Coriolis flowmeter, solid volume fraction, Gaussian Process Regression.**

I. INTRODUCTION

SOLIDS conveyance through pipes are encountered in many industries around the world, mostly for the economic advantages of this model of transportation [1]. A typical example of such a system is slurry transportation. Slurry is a mixture of solid particles with liquid and is typically used to convey solids by carrier liquid, such as coal-water slurry, paper pulp, drilling mud and clays [1, 2]. In the broad variety of environments where solids hydro transport is applied, different solid–liquid mixtures are produced and conveyed primarily through pressurized pipes. Water is a typical carrying liquid, but the carried solid particles can vary greatly, from very fine to very coarse and from very heavy to very light [3]. Hydraulic transport of solids is of importance in many industries, for instance, chemical (e.g. hydrochloric acid), pharmaceutical (e.g. passivation process), petroleum (e.g. hydraulic fracturing), mining (e.g. drilling mud, clays and fine limestone) as well as manufacturing (e.g. production of cement, brick, mortar, concrete or glass) industries. Slurry flow is widely seen in oil refineries as well for the transportation of oil-sand from mines to the extraction facilities [4]. In addition, slurry transportation is used in carbon capture and storage facilities for safe storage of CO_2 in ocean sub-seabed sites in the form of clathrate hydrates [5, 6].

In a slurry flow, the two phases (liquid and solid) interact with each other while flowing through a conduit, which significantly affects the behavior of the mixture [3]. The physical characteristics and behaviors of slurry flow depend on several factors such as size, concentration and distribution of solid particles as well as turbulence level, velocity, temperature and viscosity of the liquid carrier. Moreover, the diameter and orientation conditions of the pipe through which the mixture flows also influence its physical characteristics [4]. Depending on these factors, slurry flow regimes in a pipe can vary. Typical flow regimes include homogeneous, heterogeneous, heterogeneous with moving bed and stationary bed, etc. [3, 7]. Besides, slurry flow in a pipeline is different from liquid flow; a liquid of low viscosity can flow (although at slow speeds) in both laminar and turbulent flow, whereas for a slurry, the mixture must flow at a velocity above a critical value to avoid settling of solid particles [8]. All of these factors made slurry a very complex flow and has attracted considerable attention of many investigators across the world for many years.

In highly demanding industrial processes, accurate measurement of solid-liquid two-phase flow is essential to realize flow quantification, operation monitoring, process optimization and product quality control [9]. Therefore, significant efforts have been devoted to address the challenges of slurry flow metering over the past few decades. As conventional flow measurement techniques, acoustic sensors [9], differential pressure devices incorporating pressure transducers [10] or venturi meters [11] have been used for slurry flow measurements. However, these methods have some limitations, for instance, in acoustic methods the external noise negatively affecting the measurement performance or blockage at the constricted area of a venturi meter. A combination of an Electromagnetic Flowmeter (EMF) with electrical resistance tomography for slurry flow measurement was attempted in [12]. However, the flowrates obtained by the EMF should be corrected by considering the slip velocity [12]. Besides, the working principle of EMF is based on Faraday's law of

Manuscript submitted July 31, 2023 *(Corresponding author: Yong Yan).*

W. S. Chowdhury and Y. Yan are with the School of Engineering, University of Kent, Canterbury, CT2 7NT, U.K. (e-mail: y.yan@kent.ac.uk).

M.-A. Coster-Chevalier and J. Liu are with KROHNE Ltd. Wellingborough NN8 6AE, U.K.

electromagnetic induction, hence, EMF is only able to sense electrically conductive fluid medium. Other tomography-based techniques such as magnetic induction [13], electrical capacitance [14] and electrical impedance [15] have also been used for two phase (solid-liquid) flow measurement. However, for tomography-based methods the measured electrical properties are always sensitive to changes in fluid dielectric properties as well as flow regimes. Frequent online calibrations are required in order to offer accurate flow measurement results, which would limit the application of tomography techniques into real-world industrial processes.

Coriolis flowmeters have been in use for mass flow measurement of single-phase flows for decades. They are the most accurate single-phase mass flow metering devices, with the benefit of offering multiple outputs, including direct measurement of mass flowrate, density, temperature etc. [16]. Since volumetric flowrate can be sensitive to process conditions, mass flowrate measurement has become more favorable, particularly in highly demanding applications [16]. The potential extension of Coriolis flow metering technology from single-phase flows to multiphase flows has received considerable attention over the past few years. Coriolis flowmeters have been used for slurry flow metering as well [5, 17, 18]. However, the primary limitation of this technique is the degradation of accuracy while measuring multiphase flows. Phase decoupling [19], compressibility [20], asymmetric damping [21] and velocity profile [22] are identified as the sources of measurement errors. Among them, phase decoupling effect is the most common and significant source that leads to measurement inaccuracies and it is a negative error [19]. Theoretical studies of this error for different types of mixtures (including slurry) flowing through Coriolis tubes are discussed in several reports [19, 21]. Although, these studies provide theoretical treatments of the error, there is lack of practical implementation in case of slurry flow measurement. With the rapid development of artificial intelligence and machine learning algorithms, data-driven models have shown a potential to assist Coriolis flowmeters for satisfactory multiphase flow metering [23, 24]. Data-driven models such as Support Vector Machine (SVM), Artificial Neural Network (ANN) have been implemented for gas-liquid flow measurement using Coriolis flowmeters [24, 25].

This study aims to extend the Coriolis flow metering technology for two-phase slurry flow measurement by incorporating data-driven models, including SVM, ANN and Gaussian Process Regression (GPR). There has been limited literature in this area of research. In this study, the performance of Coriolis flowmeters while measuring slurry flow is evaluated through extensive experimental tests on a two-inch bore purpose-built slurry flow test rig. This study examines for the first time the effect of flowmeter tube geometry and orientation conditions leading to measurement inaccuracies by installing two Coriolis flowmeters (KROHNE OPTIMASS 6400 S50) in upward and downward orientations. The concept along with preliminary results were initially reported at the 2023 IEEE International Instrumentation and Measurement Technology Conference [26]. In this extended paper, new data were acquired under a wider range of mass flowrates (5435 - 18582 kg/h) and Solid Volume Fractions (SVFs) 0 - 3.3%. The original errors along with additional factors that lead to the errors including density difference, asymmetry and damping are practically examined and reported. The behaviors of Coriolis flowmeters while measuring slurry flow as well as practical evaluation of the proposed mass flow metering system is discussed in detail. An augmented dataset is also generated to evaluate the generalizability of data-driven models. In addition, comparative analysis is conducted to evaluate the performance of data-driven models under seen and unseen conditions.

II. Methodology

A. Overall Measurement System

Fig. 1 illustrates the basic principle and structure of the proposed slurry flow measurement system using a Coriolis flowmeter. The flowmeter provides apparent mass flowrate, density, temperature etc. information about the mixture flowing through the tubes [16]. Although, some of these parameters (e.g. mass flowrate, density) are erroneous under two-phase/multiphase conditions, they still reflect the true mixture mass flowrate and SVF to some extent. These parameters are used to determine the expected mass flowrate of mixture by incorporating data-driven models based on SVM [25], ANN [25] and GPR [27]. These regression based models are computationally less expensive. They are used in this study because the observed original errors of Coriolis flowmeters for mass flowrate measurement of slurry are, to some extent, linear and repeatable. The error trends are discussed in Section III. D.

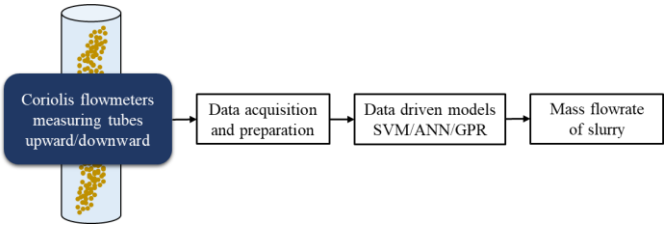

Fig. 1. Principle and structure of the proposed slurry mass flowrate measurement system.

B. Support Vector Machine (SVM)

SVM models are one of the most popular and widely implemented data driven algorithms which perform linear regression in a high dimensional feature space and tend to reduce model complexity. The type of SVM model implemented in this research is regression for the measurement of mass flowrate of slurry. As shown in Fig. 2, the input features $x = \{x_1, x_2, \cdots, x_n\}$ are mapped into an L-dimensional feature space. The feature space consists of kernel function $k(x, x_n)$. The model then performs linear regression by using kernel function values, weights $u = \{u_1, u_2, \cdots, u_L\}$ and biases to predict mass flowrate of slurry. Here, n and L denote number of input features and nodes, respectively. SVM regression is

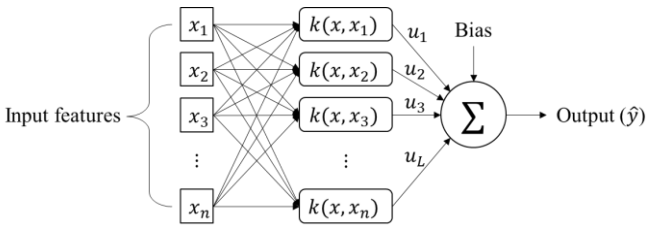

Fig. 2. Structure of SVM [25].

considered as a nonparametric technique because it relies on kernel functions. The kernel technique is useful to minimize the computational complexity of the input data which is comprised of several statistical features in the original space [25].

C. Artificial Neural Network (ANN)

The ANN model is developed by training a network of neurons to represent the inherent relationship between the input data and the intended measurand on output. The ANN model (Fig. 3) consists of an input layer, a single-hidden layer and an output layer. This three-layer feedforward neural network is trained based on the backpropagation learning method. The nodes present in the hidden layer receive values from the input layer and generates a quantitative value thorough a pre-defined activation function. An activation function in the ANN model performs the complex computation in the hidden layer and then transfers the outcome to the output layer to generate the predicted mass flowrate of slurry. An activation function is used to introduce the non-linearity in the model [25].

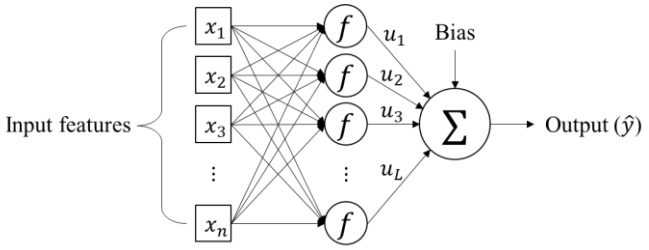

Fig. 3. Structure of ANN [25].

D. Gaussian Process Regression (GPR)

GPR is used to estimate the errors since it does not require a fitting function to be declared in exact form. It uses a covariance matrix that reflects correlation between the features of the sample in Gaussian Process (GP). It generates a confidence interval along with the predicted output. Thus, GPR shows good fitting ability. The GPR model is discussed in detail in [27].

A GP is a collection of limited number of random variables which have consistent joint Gaussian distributions. That is, for any input feature x from the feature matrix $x = \{x_1, x_2, \dots, x_n\}$, its probability distribution function $f(x)$ follows the Gaussian distribution. Hence, the GP is specified as:

$$f(x) \sim GP(\mu(x), k(x_n, x_n)) \tag{1}$$

where $\mu(x)$ is the mean function and $k(x_n, x_n)$ is the kernel function created by the covariance matrix.

In GPR the Bayesian principle is used to construct a predictive model. Where the undermined parameters of kernel function are iteratively achieved to determine the optimal parameters. Based on that a prior distribution is established for the training samples. Then the joint posterior distribution of training samples y and estimated output $\hat{y}$ for the test samples ($\hat{x}$) are established:

$$\begin{bmatrix} y \\ \hat{y} \end{bmatrix} \sim N\left(0, \begin{bmatrix} K(X,X) & K(X,\hat{X})^T \\ K(X,\hat{X}) & K(\hat{X},\hat{X}) \end{bmatrix}\right) \tag{2}$$

Where $N()$ indicates a normal distribution, T denotes the transpose matrix. $K(X,X)$, $K(\hat{X},\hat{X})$ and $K(X,\hat{X})$ represents the covariance matrices among inputs from training set (already observed points), test set (new input points) as well as training and test sets, respectively. The following equations give the covariance matrices:

$$K(X,X) = \begin{bmatrix} k(x_1,x_1) & k(x_1,x_2) & \cdots & k(x_1,x_n) \\ k(x_2,x_1) & k(x_2,x_2) & \cdots & k(x_2,x_n) \\ \vdots & \vdots & \ddots & \vdots \\ k(x_n,x_1) & k(x_n,x_2) & \cdots & k(x_n,x_n) \end{bmatrix} \tag{3}$$

$$K(X,\hat{X}) = [k(x_1,\hat{x}) \quad k(x_2,\hat{x}) \quad \cdots \quad k(x_n,\hat{x})] \tag{4}$$

$$K(\hat{X},\hat{X}) = k(\hat{x},\hat{x}) \tag{5}$$

The joint posterior distribution of estimated value $\hat{y}$ can be given as:

$$P(\hat{y}|\, x, y, \hat{X}) \sim N(f|0, K(X,X)) \tag{6}$$

Finally, the mean distribution is used as the estimated output.

$$\hat{y} = K(X,X)K(X,X)^{-1}y \tag{7}$$

As a key to GPR, the kernel function determines the property of GP, and is used to obtain covariance matrix. The choice of a kernel is based on assumptions such as smoothness and likely patterns to be expected in the data [28]. Common kernel functions includes Rational Quadratic Kernel (RQK), Exponential Kernel (ExK), Squared Exponential Kernel (SEK) and Matern 5/2 Kernel (M5/2K), which are defined as follows:

$$k_{RQK}(x_i, x_j) = \sigma^2\left(1 + \frac{r^2}{2\alpha l^2}\right)^{-\alpha} \tag{8}$$

$$k_{ExK}(x_i, x_j) = \sigma^2 exp\left(-\frac{r}{2l^2}\right) \tag{9}$$

$$k_{SEK}(x_i, x_j) = \sigma^2 exp\left[-\frac{r^2}{2l^2}\right] \tag{10}$$

$$k_{M5/2K}(x_i, x_j) = \sigma^2\left(1 + \frac{\sqrt{5}r^2}{\sigma} + \frac{5r^2}{3\sigma^2}\right) exp\left(-\frac{\sqrt{5}r}{\sigma}\right) \tag{11}$$

r is defined as:

$$r = \|x_i - x_j\| \tag{12}$$

α is a scale-mixture parameter ($\alpha > 0$), σ and l are height and length scale parameters, respectively, x_i and x_j represents two points in feature space, respectively.

In order to determine the optimal kernel function a comparative analysis is carried out in Section III based on the Root Mean Square Error (RMSE).

$$RMSE = \sqrt{\frac{1}{m}\sum_{i=1}^{m}(y_i - \hat{y}_i)^2} \tag{13}$$

where m is the number of training samples, y_i and $\hat{y}_i$ are the reference and predicted mass flowrates of i -th sample, respectively.

III. Experimental Results and Discussion

A. Test Facility and Conditions

A laboratory-scale 50 mm bore sand-water slurry flow test rig was designed and constructed to acquire the experimental data of this study. Figs. 4 and 5 illustrates the schematic and physical implementation of the test rig, respectively. In order to investigate the effect of Coriolis measuring tubes orientation for slurry flow metering two deeper V-shaped Coriolis flowmeters (KROHNE OPTIMASS 6400 S50) with their measuring tubes upward and downward orientations are mounted on the same pipeline. Three tanks: slurry tank (1500 liters), weighing tank (300 liters) and

buffer tank; and three pumps: main pump (centrifugal, rated 5.5 kW), secondary pump and agitator (0.37 kW) are also there in the rig. The slurry tank is used to store sand-water and the agitator is placed over the tank to create dilute sand-water slurry. A weighing system with uncertainly lower than the flowmeters under test is used to acquire the reference mixture mass readings. The buffer tank is used for sand-water separation and a secondary pump is there to feed the separated water back into slurry tank. All of these pumps, flowmeters and tanks are connected through a main circulation loop pipeline. The main pump is used to allow the slurry to flow throughout the pipeline homogenously. A number of valves are also fitted on the rig to regulate the direction of slurry flow. Two motor control inverters are in place to control the frequencies of main pump and agitator to achieve the desired mass flowrate and SVF, respectively. Fig. 6 illustrates the test matrix, which consists of seven different mass flowrates (5435, 8239, 10743, 13074, 15186, 17045 and 18582 kg/h) over SVF

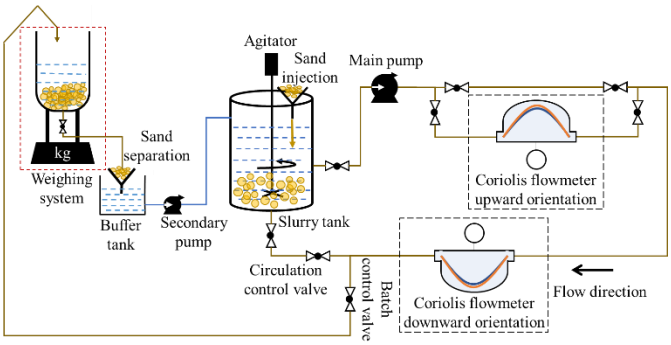

Fig. 4. Schematic of the sand-water two-phase slurry test rig.

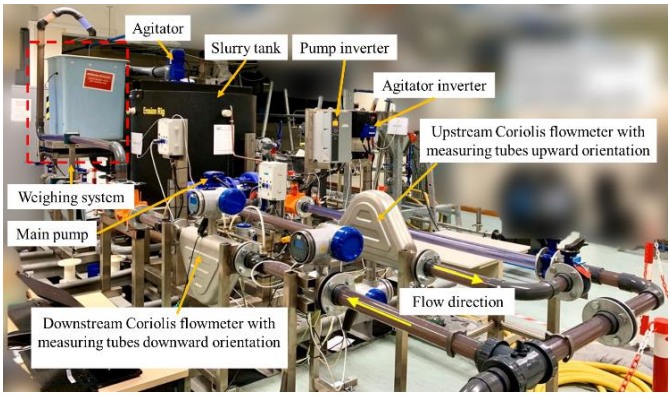

Fig. 5. Photo of the two-phase slurry test rig.

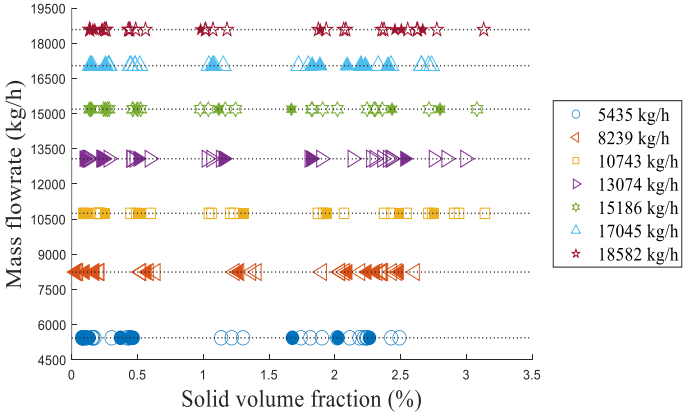

Fig. 6. Test matrix of two-phase slurry mass flow measurement (empty markers for training and filled markers for testing).

0-3.3%. The measurements under each test conditions were repeated for five times. In this research 70% of data from the test matrix are used to train the data-driven models whereas the remaining 30% for testing the models. Training and test conditions are shown in Fig. 6 as empty and filled markers, respectively.

B. Sensor Features

Several features, including apparent mass flowrate, apparent density, process temperature, water density, sensors A & B amplitudes, tube frequency, two phase signal, drive level and time shift were obtained from each of the two Coriolis flowmeters. Additional features such as: SVF ($\alpha_{s,app}$) , asymmetry (*ASY*) and damping (P_d) were determined as follows:

$$\alpha_{s,app} = \frac{\rho_{app} - \rho_w}{\rho_s - \rho_w} \times 100\% \quad (14)$$

$$ASY = \frac{S_B}{S_A} \quad (15)$$

$$P_d = \frac{I_{dr}}{(S_A + S_B)/2} \quad (16)$$

where ρ_s, ρ_w, ρ_{app}, S_A, S_B and I_{dr} are sand (2680 kg/m^3), water (~998 kg/m^3), mixture densities, Sensor A & B amplitudes and drivel level, respectively.

The reference mass flowrate is obtained by dividing the weighing scale reading with operating time and is used to calculate the relative error ($E_{\dot{m}}$) (Eq. 17).

$$E_{\dot{m}} = \frac{\dot{m}_{app} - \dot{m}_{ref}}{\dot{m}_{ref}} \times 100\% \quad (17)$$

where $\dot{m}_{app}$ and $\dot{m}_{ref}$ are the apparent and reference mass flowrates of slurry, respectively.

TABLE I MODEL TRAINING FEATURES AND THEIR PHYSICAL DEFINITIONS

ID	Features	Physical definition
x_1	Apparent mass flowrate (kg/h)	The mass flowrate reading from upward or downward Coriolis flowmeter based on the calibration cahracteristics for single-phase flows.
x_2	Apparent SVF (%)	Solid volume fraction obtained from Eq. (14).
x_3	Process temperature (°C)	Fluid temperature reading from the Coriolis flowmeters.
x_4	Water density (kg/m^3)	Water density determined from current process temperature using IAPWS R7-97 method [29].
x_5	Two phase signal	Indication of the presence of a second phase in the tube(s).
x_6	Drive level (%)	The current amplitude of the driver output for the vibration of Coriolis tubes. It is the ratio between the input current and maximum available current of 85 mA.
x_7	Asymmetry	The ratio between the amplitudes of the two sensor outputs, Eq. (15).
x_8	Damping	The ratio between drive level and sensor voltage, Eq. (16).
y	Reference mass flowrate (kg/h)	Obtained from the weighing scale readings and Coriolis flowmeter operating time.
$\hat{y}$	Predicted mass flowrate (kg/h)	Output of a data-driven model for the measurement of slurry mass flowrate under two-phase flow conditions.

Table I summarizes the model training features and their physical definitions. These features were obtained through measuring or transforming the internal parameters of the two

Coriolis flowmeters and no addition sensors or equipment were involved.

C. Behavior analysis of Coriolis flowmeters while measuring slurry flow

This section discusses about how the two Coriolis flowmeters (upward and downward) reacted while measuring slurry flow. A Coriolis flowmeter is a delicately designed vibrating system. The excellent symmetry and perfect balance between the measuring tubes are vital to achieve accurate flow measurement. However, under two-phase flow conditions, the second phase (solid particles) typically appears as a non-continuous phase, which is usually dispersed or not uniformly distributed in the fluid, giving rise to the asymmetries along the Coriolis tube. Concerning a Coriolis flowmeter with twin bent tubes, the mixture flow may not be equally split into each measuring tube, resulting in imbalance. Once flowmeters are not symmetric and balanced, the sensor signal is likely to be distorted by the external influences. Particularly, when the flow velocity becomes low, the changes in flow regime and the gravity effect on particles distribution would bring the extra asymmetry and damping errors of Coriolis flow metering.

- **Two Phase Signal:** This is a signal from the Coriolis flowmeter indicating the presence of a second phase, Fig. 7 (a) and (b) illustrates the readings of two-phase signals from upward and downward Coriolis flowmeters, respectively. It is observable that, when SVF is below 1%, the two-phase signal is insignificant. However, as SVF is higher, there is a gradual growth in the two-phase signal strength. This is because, as SVF gets higher, the presence of second phase is becoming more significant.
- **Asymmetry:** This usually refers to the uneven distribution of solid particles at inlet and outlet of the Coriolis measuring tubes, resulting in a difference between the two sensor signals. Fig. 7 (c) and (d) illustrates the degree of asymmetry that the upward and downward Coriolis flowmeters experiences while measuring slurry flow under the experimental conditions, respectively. It is evident that asymmetry is higher (1.017 – 1.019) in the upward orientation

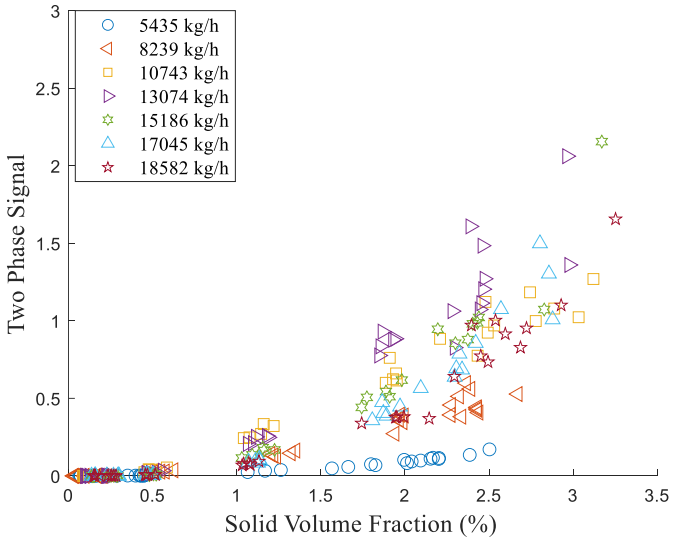

(a) Two phase signal - measuring tubes upward

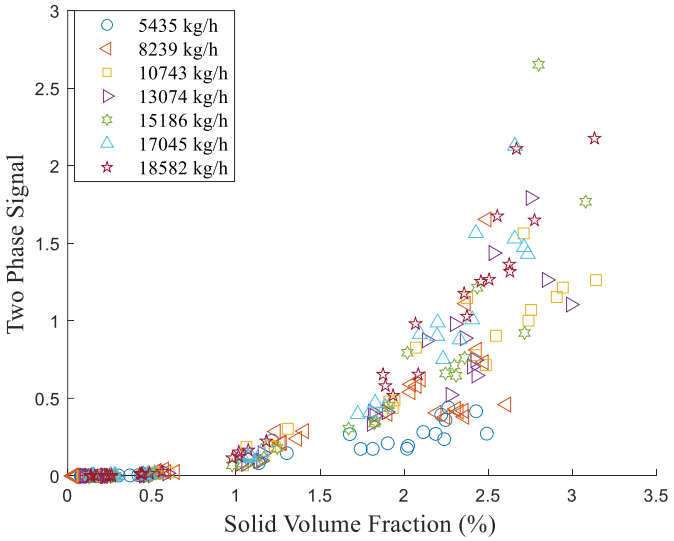

(b) Two phase signal - measuring tubes downward

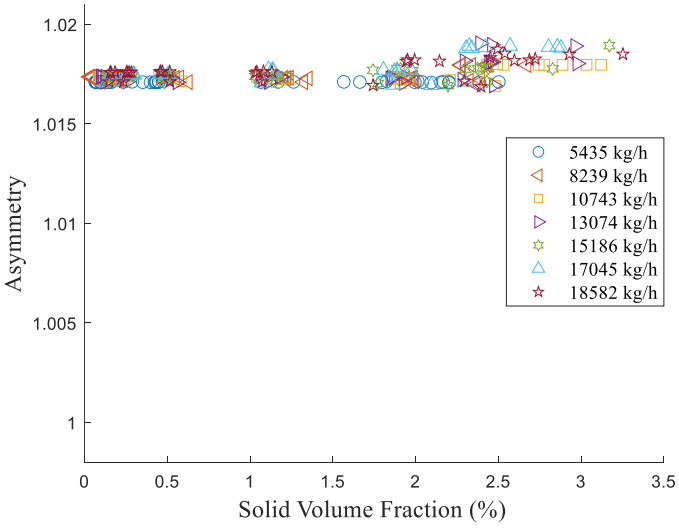

(c) Asymmetry - measuring tubes upward

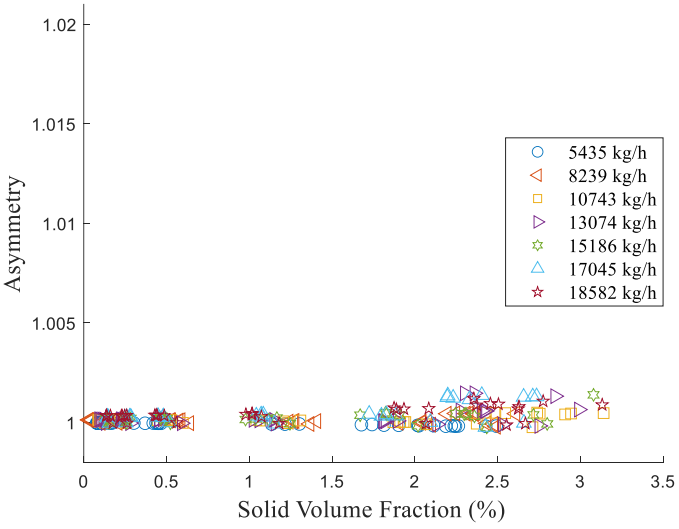

(d) Asymmetry - measuring tubes downward

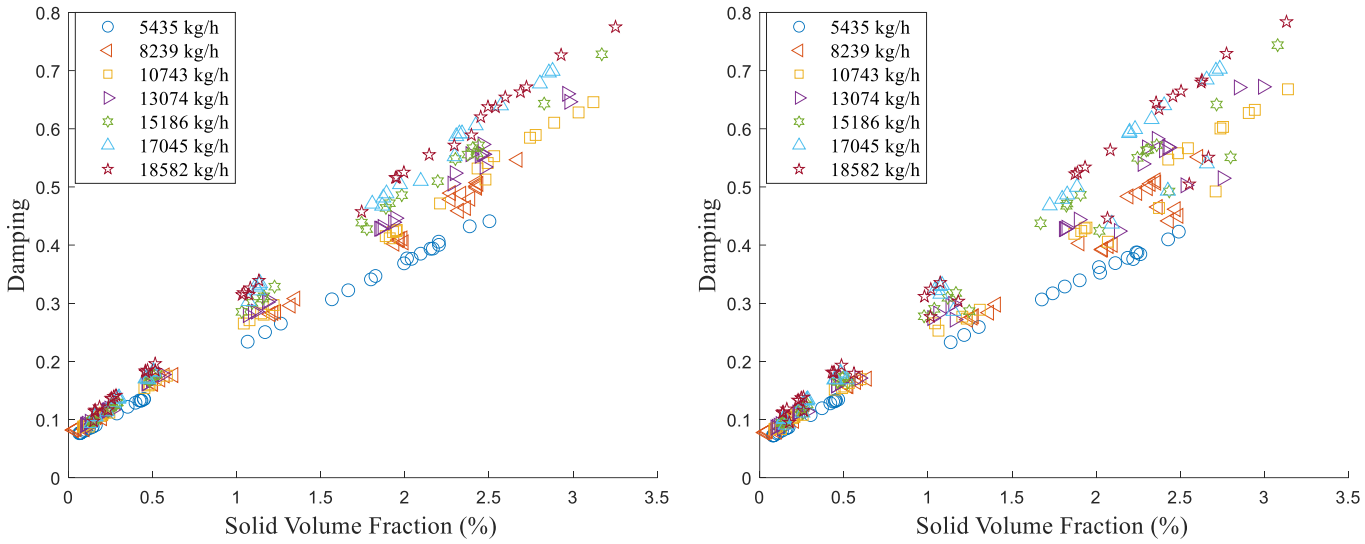

(e) Damping - measuring tubes upward (f) Damping - measuring tubes downward

Fig. 7. Behavior analysis of the Coriolis flowmeters while measuring slurry flow.

and lower (0.9998 - 1.0015) in the downward orientation of Coriolis measuring tubes. It should be mentioned that these asymmetry readings are flowmeter-specific and the trend may not be applicable to other Coriolis flowmeters under the same orientation conditions.

- **Damping:** Generally damping refers to as the decay in vibration amplitudes of Coriolis tube oscillation. A high damping of a free oscillation system suggests rapid decay in the amplitude of the Coriolis tube oscillation. Fig. 7 (e) and (f) demonstrates the effect of damping that the upward and downward flowmeters experiences while measuring slurry flow, respectively. It can be seen from Fig. 7 that damping has strong correlation with SVF.

D. Analysis of original errors

Fig. 8 illustrates the original errors of the two Coriolis flowmeters under all test conditions. For both flowmeters almost all errors are negative, which confirms that phase decoupling is the most significant source of error. The results also reveal a strong correlation between SVF and relative error, and the higher the SVF the higher the error. Moreover, the worst error of the downward meter (-3.4%) is higher than that of the upward meter (-2.4%). This is because sand particles get accumulated inside the Coriolis measuring tubes and affect the flowmeters density readings.

Fig. 9 compares the density readings from both flowmeters for a single batching operation. It is observable that, for the initial seven seconds, the density reading from the upward flowmeter stays close to water density (~998 kg/m^3). This is because, for the upward flowmeter more sand tends to settle at the inlet side of the deeper V-shaped tubes due to gravity effect, which adds extra damping on the inlet side and consequently causes additional positive errors in mass flowrate. There is a sharp peak at about 10s when the accumulated sand moves through the upward flowmeter tubes and the density reading returns to water density at the end of batching.

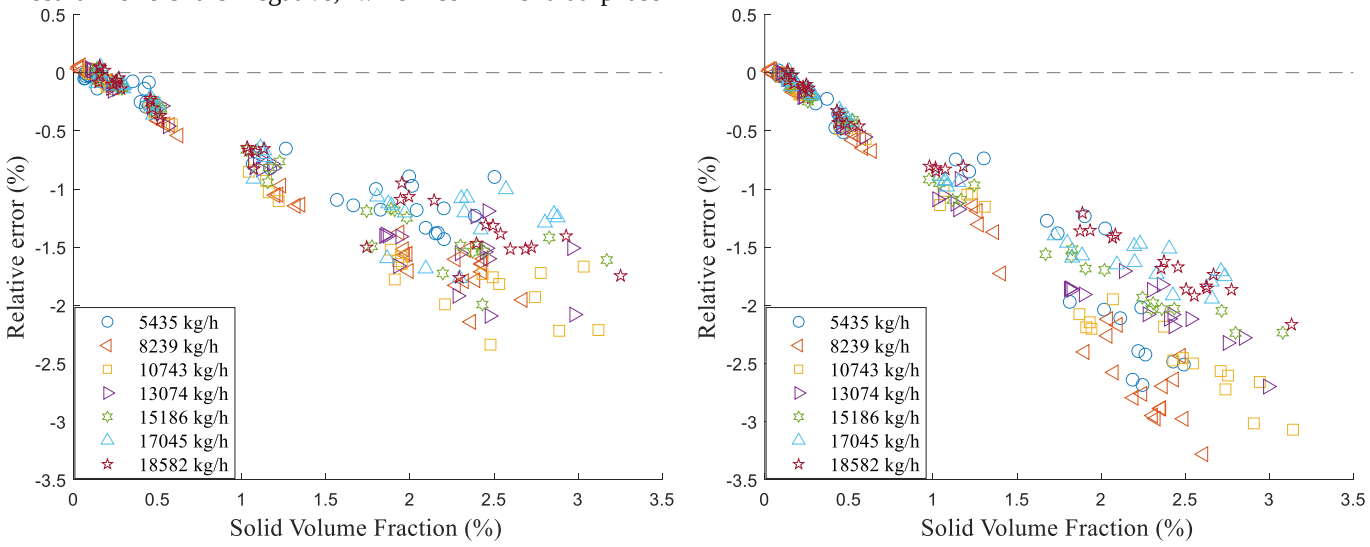

(a) Measuring tubes upward (b) Measuring tubes downward

Fig. 8. Original errors of the Coriolis flowmeters without the correction model.

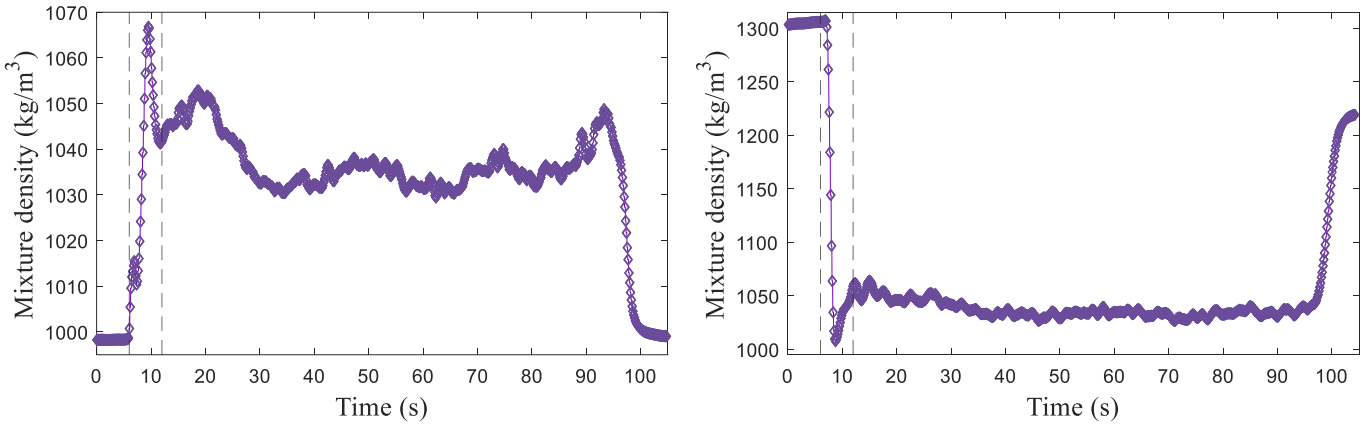

(a) Measuring tubes upward (b) Measuring tubes downward

Fig. 9. Difference in initial density readings of the Coriolis flowmeters

In contrast, the initial density reading for the downward meter is significantly higher (~1300 kg/m^3) because of sand particles accumulation at the bottom of the tubes, resulting in more damping imposed on the outlet as well as extra negative errors. Hence, there is a sharp decline in density readings at about 10s when the accumulated sand moves from the downward flowmeter tubes and the density reading goes back up again at the end of batching.

As a result, for the upward meter, the additional positive error due to asymmetry cancels out a part of the negative error due to decoupling effect, whereas for the downward meter the negative error due to asymmetry introduces additional error to the decoupling error. Therefore, the upward installation orientation would produce smaller error than the downward orientation. Another possible source of error is imbalance, arising when the mixture flow is not equally split between the two measuring tubes. It is evident that, apart from the density differences between the phases in the mixture flow, tube geometry and installation orientations also affect the flowmeter behavior, and the upward installation orientation is favorable for slurry flow measurement compared to the downward orientation.

E. Implementation of data-driven models

While developing the data-driven models, it is crucial to determine the optimal parameters of the models to achieve good generalization capability.

For the ANN and SVM models the number of nodes in the hidden layer is determined with the method discussed in [30]. The range of the number of nodes is determined from:

$$L \leq 2m + 1 \tag{18}$$

$$L = \frac{n}{m+1} \tag{19}$$

where L, m and n are the numbers of nodes, training samples and features, respectively. Although eq. (18) and eq. (19) provide only a range of L for SVM and ANN models, the exact number of L is determined by trial-and-error for a given dataset. Table II shows the number of nodes of the SVM and ANN models. Moreover, the ANN model with the Rectified Linier Unit (ReLU) activation function outperforms other functions in terms of RMSE. Hence, the ReLU activation function is used in this study to develop the ANN model. For the SVM model, quadratic kernel function in conjunction with the Sequential Minimal Optimization (SMO) solver has been proven to be more effective than other versions of SVM. Thus, these parameters are used while developing the SVM models.

TABLE II PARAMETERS OF ANN AND SVM MODELS

Parameter	ANN	SVM
Type of model	Regression	Regression
Activation / kernel function	ReLU	Quadratic
No. of Hidden layers	1	1
Number of hidden nodes	10	10
Learning rate	0.001	0.001

Since, kernel functions in a GPR model play an important role in calculating the similarities between two signals from the sensor, it is crucial to determine the most suitable one prior to model training. As discussed in Section II four types of kernel functions (RQK, ExK, SEK and M5/2K) are typically used in GPR. In this study, four GPR models are implemented with all the four kernel functions. Fig. 10 shows the performances of the four kernel functions based on RMSE. It is observable that M5/2K, RQK and SEK performs almost similar, however, SEK exhibits lowest RMSE (0.092) while testing compared to M5/2K (0.095) and RQK (0.094). SEK exhibits the lowest RMSE because the GP with SEK has mean-square derivatives of all orders, and thus the GPR is relatively smooth [28]. Therefore, SEK is used in this study for the correction model.

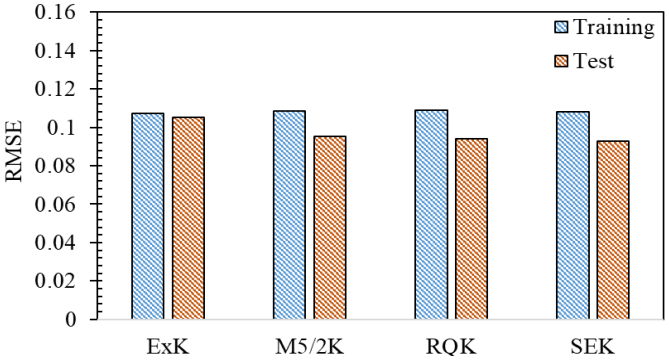

Fig. 10. Performance analysis of GPR model for different kernel functions.

F. Slurry mass flowrate correction

In order to compensate the significant errors as illustrated in Fig. 8, three data-driven models based on SVM, ANN and GPR are used in this study for each orientation.

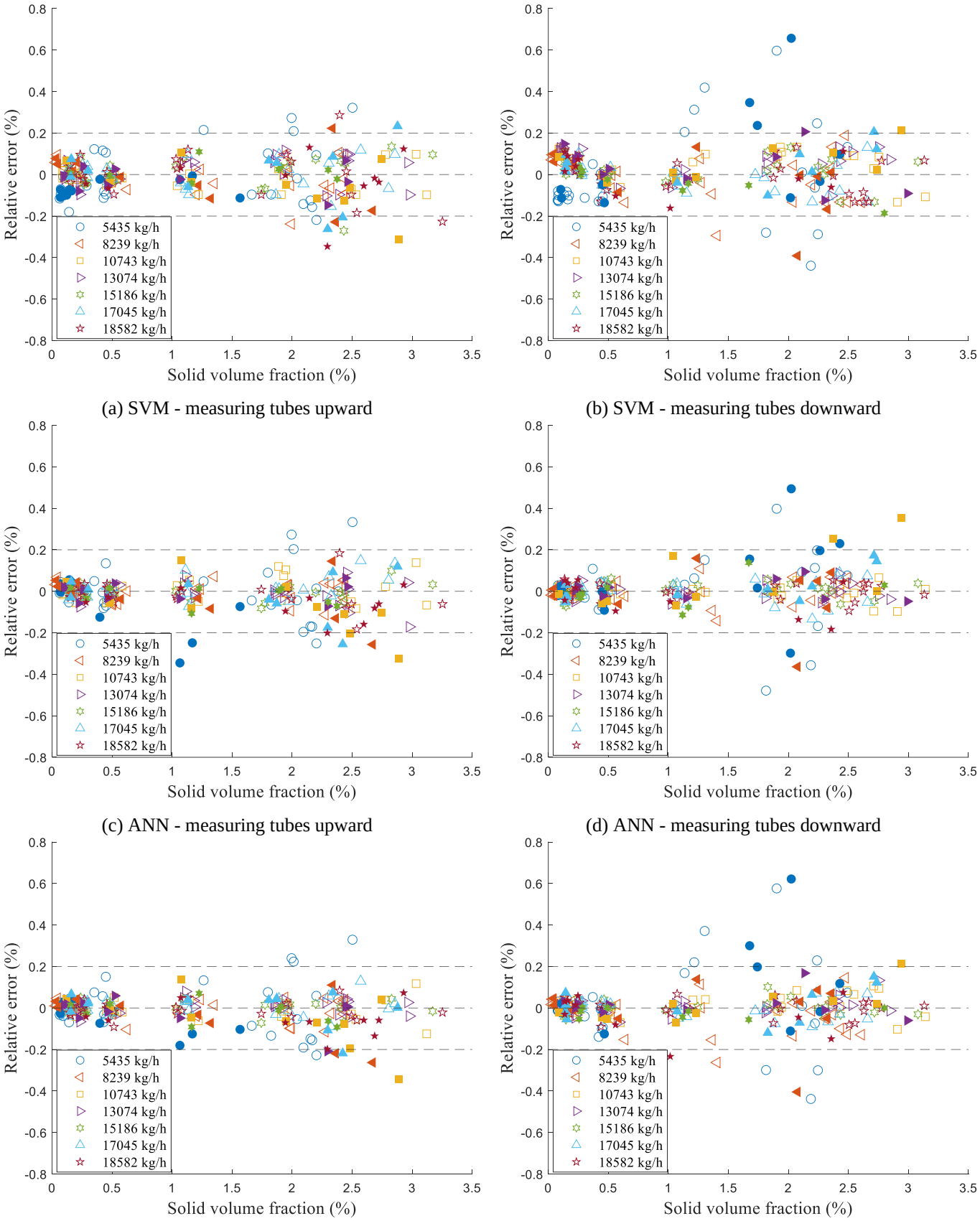

(a) SVM - measuring tubes upward

(b) SVM - measuring tubes downward

(c) ANN - measuring tubes upward

(d) ANN - measuring tubes downward

(e) GPR - measuring tubes upward

(f) GPR - measuring tubes downward

Fig. 11. Relative error in slurry mass flowrate measurement with the data-driven models (empty markers from training and filled markers from testing dataset)

Fig. 11 shows the relative errors of all the six models for upward and downward installations of the flowmeters, respectively. For both orientations the models are able to limit the errors within ±0.2% under all test conditions for the following percentages of data: SVM 93.5% and 93.5% (Fig. 11 (a) and (b)), ANN 96% and 95% (Fig. 11 (c) and (d)) and GPR 97% and 95.5% (Fig. 11 (e) and (f)), respectively. The GPR models outperform all other models in effectively predicting the mass flowrate of slurry.

The models were trained and tested for seven different mass flowrates (5435, 8239, 10743, 13074, 15186, 17045 and 18582 kg/h) and SVF ranging between 0-3.3%. However, the performance of the models under unseen conditions (e.g. 6000 or 16500 kg/h) are yet to be assessed. Therefore, a data augmentation technique is used in this study to generate unseen conditions data. Data augmentation is a common practice in Machine Learning to generate additional data from the original dataset [31]. It is mostly used for model training when the number of data samples are low. However, in this study the augmented dataset is used for model performance evaluation under unseen conditions. A random rotation technique is used to randomly select 50% of the original data samples and shuffle them randomly for ten times. The augmented dataset is then achieved by taking an average of them. The unseen condition data are achieved by omitting the samples that are identical to

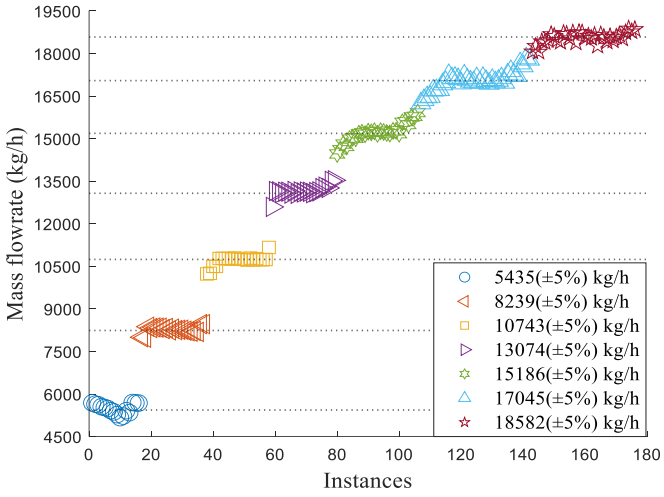

Fig. 12. Mass flowrates achieved from the augmented dataset with ±5% deviation.

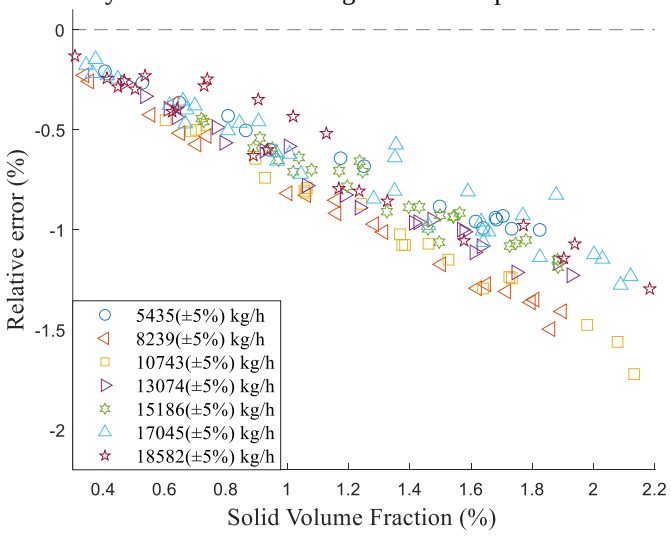

(a) Original errors - measuring tubes upward

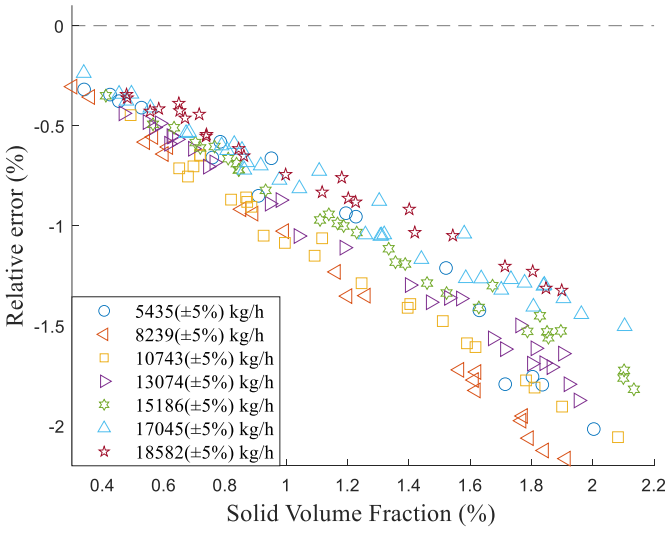

(b) Original errors - measuring tubes downward

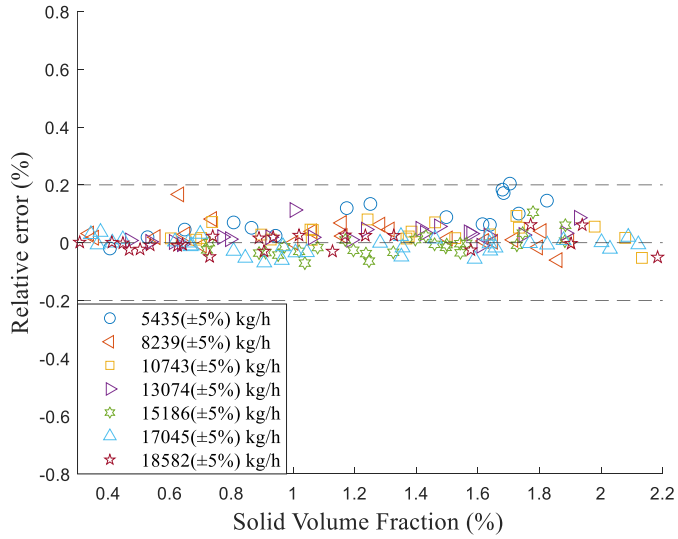

(c) SVM -measuring tubes upward

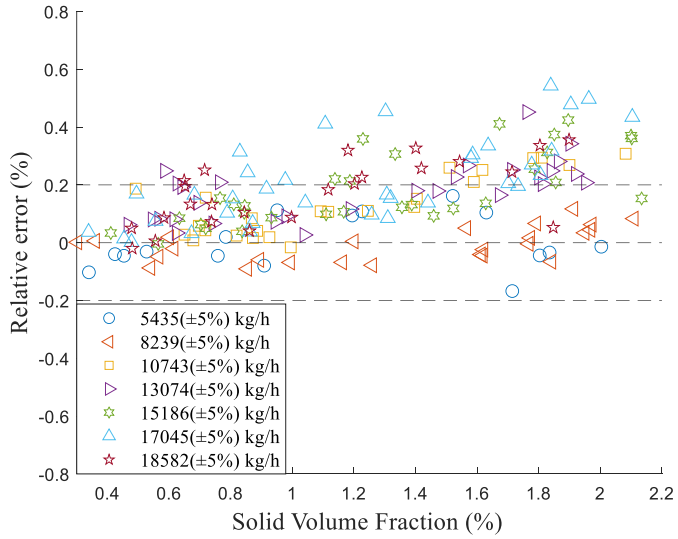

(d) SVM - measuring tubes downward

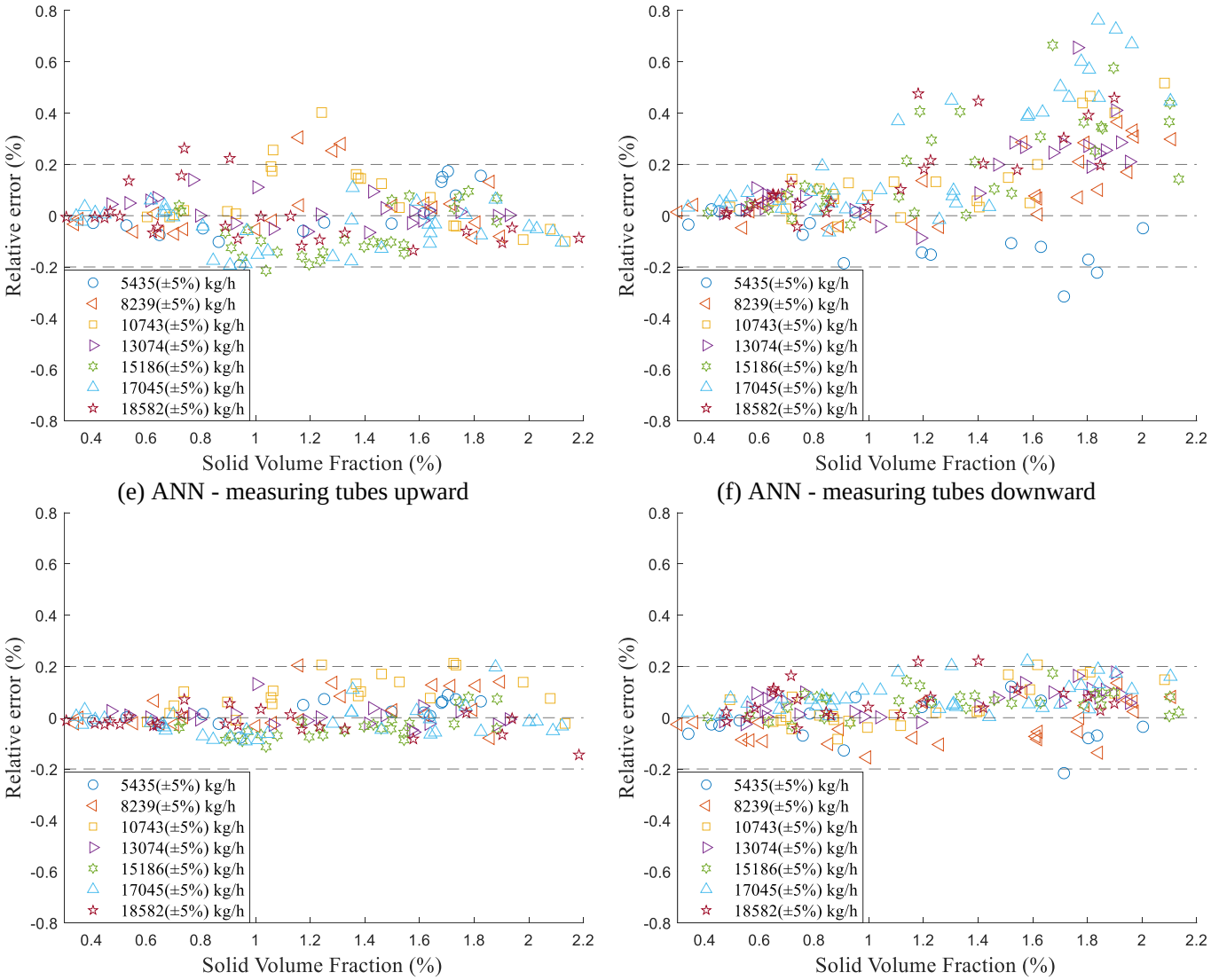

(e) ANN - measuring tubes upward (f) ANN - measuring tubes downward

(g) GPR - measuring tubes upward (h) GPR - measuring tubes downward

Fig. 13. Relative error in slurry mass flowrate measurement with and without the data-driven models for unseen conditions dataset.

the original samples. Hence, the volume of data on the augmented dataset is reduced to 176 with a deviation of ±5% from the original data and SVF 0.35-2.2% for all the seven mass flowrates. Fig. 12 shows the mass flowrates and Fig. 13 (a) and (b) illustrates the errors achieved through the data augmentation technique. This further validation of the data-driven models is useful because, in real life scenario, it is highly unlikely that the mass flowrates or SVF will be the same as the models are trained with. As a result, how the models will perform under unseen conditions needs to be evaluated. As shown in Fig. 11, the models can effectively minimize the original errors within ±0.2% over SVF 0-2.2%. Since, the SVF range in the augmented dataset is narrower (0.35 – 2.2%) than that in the original dataset, the models should have been able to limit the errors within ±0.2%. However, Fig. 13 indicates that the SVM and ANN models deteriorate significantly for the downward meter. The GPR model has performed as expected for >98% of the augmented data within ±0.2% error range for both upward and downward orientations, and for <2% of augmented data, the GPR model deteriorates slightly. The GPR model outperforms the SVM and ANN models because of the confidence interval it generated along with the predicted mass flowrate of slurry. Any new data either from test or augmented dataset that falls within the confidence interval is effectively predicted by the GPR.

IV. Conclusion

This paper has presented a slurry mass flowrate measurement system using Coriolis flowmeters through data-driven modelling. Extensive experimental tests were conducted on a purpose-built slurry flow test rig for upward and downward orientations of the flowmeters.

- The experimental results have revealed that phase decoupling effect is the most significant source of error that a Coriolis flowmeter experiences while measuring slurry flow and the upward orientation is more favorable compared to the downward orientation for slurry flow metering.
- Apart from the density differences between multiple phases, asymmetry, damping, Coriolis tube geometry and

orientation introduce additional errors to the flowmeter readings.

- A comparative analysis between the SVM, ANN and GPR models for the prediction of mass flowrate under two-phase slurry flow conditions has suggested that the GPR models are superior to the SVM and ANN models in terms of robustness and accuracy.
- The GPR models perform well under both seen and unseen conditions while the performance of the SVM and ANN models significantly deteriorates for unseen conditions.
- For both the upward and downward orientations of Coriolis measuring tubes most of the corrected errors (>95.5% for seen conditions and >98% for unseen conditions) of the GPR models are within ±0.2%.

In comparison with the original errors, the proposed models have provided significant improvements in measurement accuracy under all test conditions. This research outcome has effectively extended the applicability of Coriolis flowmeters to two-phase slurry mass flow measurement. It should be noted that the developed data-driven models are implemented with a dataset collected on a laboratory flow test rig. The models should work effectively for practical slurry flow metering, given the actual flow conditions are within the rage of their training conditions. However, for different conditions, e.g. higher SVF% or different orientations of Coriolis tubes, the models need to be retrained.

ACKNOWLEDGMENT

The authors would like to acknowledge Dr. Jingqiong Zhang, a Research Associate from the Department of Automatic Control and Systems Engineering, University of Sheffield, for her contributions to the I2MTC 2023 conference version of this paper. Wasif Shafaet Chowdhury would like to thank the University of Kent for providing a PhD studentship that has led to this publication.

REFERENCES

[1] M. Z. Li, Y. P. He, Y. D. Liu, and C. Huang, “Effect of interaction of particles with different sizes on particle kinetics in multi-sized slurry transport by pipeline,” *Powder Technology*, vol. 338, pp. 915–930, 2018.

[2] G. V. Messa, M. Malin, and S. Malavasi, “Numerical prediction of fully-suspended slurry flow in horizontal pipes,” *Powder Technology*, vol. 256, pp. 61–70, 2014.

[3] G.V. Messa, Q. Yang, O. E. Adedeji, Z. Chára, C. A. R. Duarte, V. Matoušek, M. G. Rasteiro, R. S. Sanders, R. C. Silva, and F. J. Souza, “Computational fluid dynamics modelling of liquid–solid slurry flows in pipelines: State-of-the-art and future perspectives,” *Processes*, vol. 9, no. 9, 2021.

[4] K. J. Albion, L. Briens, C. Briens, and F. Berruti, “Multiphase flow measurement techniques for slurry transport”, *International Journal of Chemical Reactor Engineering*, vol. 9, pp.18-19, 2011.

[5] B. Prah, and R. Yun, “CO_2 hydrate slurry transportation in carbon capture and storage,” *Appl Therm Eng*, vol. 128, pp. 653–661, 2018.

[6] M. F. Costa, C. M. Teixeira, A. M. Lopes, J. P. Araújo, M. M. Dias, R. J. Santos, and J. C. B. Lopes, “Carbon capture and storage toward industrialization: a novel continuous process for the production of carbon dioxide clathrates,” *Energy Technology*, vol. 10, no. 6, Jun. 2022.

[7] Y. Faraj, and M. Wang, “ERT investigation on horizontal and vertical counter gravity slurry flow in pipelines,” *Procedia Engineering*, vol. 42, pp. 588-606, 2012.

[8] B. ’Abulnaga, *Slurry Systems Handbook*. McGraw-Hill Education, 2002.

[9] M. G. Droubi and R. L. Reuben, “Monitoring acoustic emission (AE) energy of abrasive particle impacts in a slurry flow loop using a statistical distribution model,” *Applied Acoustics*, vol. 113, pp. 202–209, 2016.

[10] C. A. Shook, R. G. Gillies, and R. S. S. Sanders, “Pipeline hydrotransport: with applications in the oil sand industry,” SRC Publication No. 11508-1E02, *SRC Pipe Flow Technology Centre*, May 2002.

[11] C.V. O’Keefe, R. Maron, J. Felix, A.M. Van Der Spek, and P. Rothman, “Non-invasive passive array technology for improved flow measurements of slurries and entrained air”, *4th International Platinum Conference: Platinum in transition ‘Boom or Bust’*, pp. 21-30, 2010.

[12] J. Y. Xu, Y. X. Wu, and Z. C. Zheng, “Measurement of solid slurry flow via correlation of electromagnetic flow meter, electrical resistance tomography and mechanistic modelling,” *Journal of Hydrodyna*mics, vol. 21, pp. 557-563, 2009.

[13] L. Ma, D. McCann, and A. Hunt, “Combining magnetic induction tomography and electromagnetic velocity tomography for water continuous multiphase flows,” *IEEE Sens J*, vol. 17, no. 24, pp. 8271–8281, Dec. 2017.

[14] D. Yang, H. Pu, H. Han, L. Liu, and C. Yan, “Huge-scale capacitance mass flowmeter in gas/solid two-phase flow with rectangular vertical pipeline,” *Measurement*, vol. 151, Feb. 2020.

[15] M. Wang, J. Jia, Y. Faraj, Q. Wang, C.-G. Xie, G. Oddie, K. Primrose, and C. Qiu, “A new visualisation and measurement technology for water continuous multiphase flows,” *Flow Measurement and Instrumentation*, vol. 46, pp. 204–212, Dec. 2015.

[16] T. Wang, and R. Baker, “Coriolis flowmeters: A review of developments over the past 20 years, and an assessment of the state of the art and likely future directions”, *Flow Measurement and Instrumentation*, vol. 40, pp. 99-123, 2014.

[17] Z. Liu, M.V. Farahani, M. Yang, X. Li, J. Zhao, Y. Song, and J. Yang, “Hydrate slurry flow characteristics influenced by formation, agglomeration and deposition in a fully visual flow loop,” *Fuel*, vol. 277, Oct. 2020.

[18] J. Zhang, T. Chen, Y. Jiao, M. Cheng, L.-L. Wang, J.-L. Wang, X.-Y. Li, and Y.-Q. Chen, “Improved activity of Ni–Mo/SiO_2 bimetallic catalyst synthesized via sol-gel method for methylcyclohexane cracking,” *Pet Sci*, vol. 18, no. 5, pp. 1530–1542, Oct. 2021.

[19] N. T. Basse, “A review of the theory of Coriolis flowmeter measurement errors due to entrained particles,” *Flow Measurement and Instrumentation*, vol. 37, pp. 107–118, 2014.

[20] J. Hemp, and J. Kutin, “Theory of errors in Coriolis flowmeter readings due to compressibility of the fluid being metered,” *Flow Measurement and Instrumentation*, vol. 17, no. 6, pp. 359–369, Dec. 2006.

[21] N. T. Basse, “Coriolis flowmeter damping for two-phase flow due to decoupling,” *Flow Measurement and Instrumentation*, vol. 52, no. May, pp. 40–52, 2016.

[22] J. Kutin, G. Bobovnik, J. Hemp, and I. Bajsić, “Velocity profile effects in Coriolis mass flowmeters: Recent findings and open questions,” *Flow Measurement and Instrumentation*, vol. 17, no. 6, pp. 349–358, 2006.

[23] O. L. Ibryaeva, V. V. Barabanov, M. P. Henry, M. Tombs, and F. Zhou, “A benchmark data set for two-phase Coriolis metering,” *Flow Measurement and Instrumentation*, vol. 72, 2020.

[24] Y. Yan, L. Wang, T. Wang, X. Wang, Y. Hu, and Q. Duan, “Application of soft computing techniques to multiphase flow measurement: A review,” *Flow Measurement and Instrumentation*, vol. 60, pp. 30-43, Apr. 2018.

[25] L. Wang, J. Liu, Y. Yan, X. Wang, and T. Wang, “Gas-liquid two-phase flow measurement using Coriolis flowmeters incorporating artificial neural network, support vector machine, and genetic programming algorithms,” *IEEE Trans Instrum Meas*, vol. 66, no. 5, pp. 852–868, May 2017.

[26] W. S. Chowdhury, Y. Yan, J. Zhang, M. -A. Coster-Chevalier and J. Liu, "Mass Flow Measurement of Slurry Using Coriolis Flowmeters," *2023 IEEE International Instrumentation and Measurement Technology Conference (I2MTC)*, Kuala Lumpur, Malaysia, pp. 1-5, May 2023.

[27] Y. Jiang, J. Jia, Y. Li, Y. Kou, and S. Sun, “Prediction of gas-liquid two-phase choke flow using Gaussian process regression,” *Flow Measurement and Instrumentation*, vol. 81, 2021.

[28] Y. Pan, X. Zeng, H. Xu, Y. Sun, D. Wang, and J. Wu, “Evaluation of Gaussian process regression kernel functions for improving groundwater prediction,” *Journal of Hydrology (Amst)*, vol. 603, Dec. 2021.

[29] “IAPWS R7-97(2012): IAPWS-IF97 Industrial Formulation for Thermodynamic Properties of Water and Steam”. [Online]. Available: http://www.iapws.org/relguide/IF97-Rev.html, Accessed: 28-Jul-2023.

[30] G. J. Bowden, G. C. Dandy, and H. R. Maier, “Input determination for neural network models in water resources applications. Part 1—

background and methodology," *Journal of Hydrology (Amst)*, vol. 301, no. 1–4, pp. 75–92, Jan. 2005.

[31] S. Demir, K. Mincev, K. Kok, and N. G. Paterakis, "Data Augmentation for time series regression: Applying transformations, autoencoders and adversarial networks to electricity price forecasting," *Applied Energy*, vol. 304, 2021.

Wasif Shafaet Chowdhury received the B.Sc. degree in computer science and engineering from the BRAC University, Dhaka, Bangladesh, in 2017 and the M.Sc. degree in advanced electronic systems engineering from the University of Kent, Canterbury, Kent, U.K., in 2019. He was a research fellow with the Information and Communication Technology Division, Bangladesh Govt. in 2018. He worked as a visiting lecturer with the BRAC University, Dhaka, Bangladesh in 2020. He is currently reading the Ph.D. degree in electronic engineering with the School of Engineering, University of Kent, Canterbury, Kent, U.K. His current research interests include multiphase flow measurement, Coriolis flowmeter technology, digital signal processing, condition monitoring, and data-driven modelling.

Yong Yan (Fellow, IEEE) received the B.Eng. and M.Sc. degrees in instrumentation and control engineering from Tsinghua University, Beijing, China, in 1985 and 1988, respectively, and the Ph.D. degree in flow measurement and instrumentation from the University of Teesside, Middlesbrough, U.K., in 1992. He was an Assistant Lecturer with Tsinghua University in 1988. In 1989, he joined the University of Teesside as a Research Assistant. After a short period of Post-Doctoral Research, he was a Lecturer with the University of Teesside from 1993 to 1996, and then as a Senior Lecturer, a Reader, and a Professor with the University of Greenwich, Chatham, U.K., from 1996 to 2004. He is currently a Professor of electronic instrumentation and the Director of Innovation at the School of Engineering, University of Kent, Canterbury, U.K. His research interests include multiphase flow measurement, combustion instrumentation, and intelligent measurement and condition monitoring.

Prof. Yan was elected as a Fellow of the Royal Academy of Engineering in 2020. He was awarded the gold medal in 2020 by the IEEE TRANSACTIONS ON INSTRUMENTATION AND MEASUREMENT as the most published author of all time from the U.K.

Marc-Antony Coster-Chevalier received the B.Sc. in Physics from Loughborough University, Loughborough, U.K. in 2011 and the PhD degree in Materials Engineering at Leicester University, Leicester, U.K. in 2018. He began working at Krohne Ltd in Wellingborough, in late 2018 as a Research and Development Engineer with research interests in Coriolis mechanical design and modelling, condition monitoring of process components and vibration/noise analysis.

Jinyu Liu received the B.Eng. degrees in electrical engineering and automation from Tianjin University, Tianjin, China, and in electronic and computer systems from the University of Kent, Canterbury, U.K., in 2012, and the M.Sc. degree in energy and sustainability with electrical power engineering from the University of Southampton, Southampton, U.K., in 2013, and the Ph.D. degree in Electronic Engineering with the University of Kent, Canterbury, U.K., in 2019. He was a research associate on a knowledge transfer partnership (KTP) project for two years from 2018 – 2020. He is currently a research engineer at R&D department, KROHNE Ltd, Wellingborough, U.K.

His research interest includes Coriolis flowmeter technology, multiphase flow measurement, condition monitoring of industrial processes, and digital signal processing.